New Journal of Physics
The open-access journal for physics

Design of bright, fiber-coupled and fully factorable photon pair sources

Luis Edgar Vicent[1], Alfred B U'Ren[1,5], Radhika Rangarajan[2], Clara I Osorio[3], Juan P Torres[3], Lijian Zhang[4] and Ian A Walmsley[4]

[1] Instituto de Ciencias Nucleares, Universidad Nacional Autonoma de Mexico, apdo postal 70-543, Mexico 04510, DF, Mexico
[2] Physics Department, University of Illinois at Urbana-Champaign, IL, USA
[3] ICFO—Institut de Ciencies Fotoniques, Mediterranean Technology Park, 08860 Castelldefels (Barcelona), Spain
[4] Clarendon Laboratory, Oxford University, Oxford OX1 3PU, UK
E-mail: alfred.uren@nucleares.unam.mx

New Journal of Physics **12** (2010) 093027 (24pp)
Received 4 March 2010
Published 15 September 2010
Online at http://www.njp.org/
doi:10.1088/1367-2630/12/9/093027

Abstract. From quantum computation to quantum key distribution, many quantum-enhanced applications rely on the ability to generate pure single photons. Even though the process of spontaneous parametric downconversion (SPDC) is widely used as the basis for photon-pair sources, the conditions for pure heralded single-photon generation, taking into account both spectral and spatial degrees of freedom, have not been fully described. We present an analysis of the spatio-temporal correlations present in photon pairs produced by type-I, non-collinear SPDC. We derive a set of conditions for full factorability in all degrees of freedom—required for the heralding of pure single photons—between the signal and idler modes. In this paper, we consider several possible approaches for the design of bright, fiber-coupled and factorable photon-pair sources. We show through numerical simulations of the exact equations that sources based on: (i) the suppression of spatio-temporal entanglement according to our derived conditions and (ii) a tightly focused pump beam together with optimized fiber-collection modes and spectral filtering of the signal and idler photon pairs, lead to a source brightness of the same order of magnitude. Likewise, we find that both of these sources lead to a drastically higher factorable photon-pair flux, compared to an unengineered source.

[5] Author to whom any correspondence should be addressed.

Contents

1. Introduction

The generation of pure single photons represents a crucial enabling step for many quantum-enhanced applications, ranging from secure quantum key distribution to quantum computation. In particular, linear optical quantum computation relies on the ability of multiple independently generated single photons to interfere (for example, see review [1]). This ability to interfere can be reduced, or even suppressed, if the single photons are described by a statistical mixture of spatio-temporal modes [2]. Single photons may be generated on-demand by individual quantum emitters, such as quantum dots (for example [3]) and color centers (for example [4]), or they may be heralded from photon pairs generated through a spontaneous parametric process, i.e. downconversion [5] and four-wave mixing [6]. In the latter case, it has been shown that single photons in *pure* quantum states may be heralded only from photon pairs with a factorable joint amplitude [2]. The phasematching and energy conservation constraints in spontaneous parametric processes imply, however, that the resulting photon pairs are, for typical source designs, highly entangled in spatio-temporal degrees of freedom. In this case, the typical solution is to resort to spatial and spectral filtering, in order to effectively generate single-mode downconverted photons. This is achieved, however, at the cost of a considerable reduction of the source brightness. The spontaneous nature of typical photon-pair sources implies that filtering can lead to prohibitively low count rates. This becomes a crucial issue for experiments relying on simultaneous generation of two or more photon pairs (for example, see [7]–[12]). An enhancement of r in the single-crystal factorable photon-pair brightness becomes an enhancement of r^2 for a dual-crystal, four-photon source and r^N for an N-crystal, $2N$-photon source. Sources leading to r values in the hundreds or the thousands could therefore represent a significant step towards practical quantum information processing implementations based on photons. In previous work, various recipes have been proposed, some of which have been demonstrated experimentally, for generation of factorable photon pairs through spontaneous parametric processes [13]–[21]. In the present paper, we investigate sources of factorable, fiber-coupled photon pairs, concentrating on the attainable brightness.

Several groups have demonstrated bright, fiber-coupled, photon-pair sources based on the process of spontaneous parametric downconversion (SPDC) (for example, see [22]–[25]). In the present work, our objective is to develop experimentally feasible techniques that may lead

to bright sources of fiber-coupled photon pairs, which also exhibit factorability in all photonic degrees of freedom. We thus present in this paper, to our knowledge, the first comprehensive analysis of the simultaneous optimization of the source brightness *and* the degree of factorability in fiber-coupled, SPDC photon-pair sources. We concentrate on non-collinear, degenerate type-I SPDC where the pump beam is allowed to be broadband, with each spectral component described, spatially, by a Gaussian beam. A monochromatic pump introduces strict spectral correlations and thus precludes photon-pair factorability [13]. Indeed, techniques for factorable photon pair generation tend to require femtosecond-duration pump pulses. We have previously shown that the relaxation of a monochromatic plane-wave pump to a broadband Gaussian beam pump, which contains a spread of k-vectors, greatly enhances the photon-pair engineering possibilities. Indeed, a source that involves: (i) a pump containing a spread of transverse k-vectors, and (ii) group velocity matching between the pump and signal/idler modes, may be exploited to achieve a specific balance of transverse and longitudinal phasematching, which can result in factorable photon pairs [27, 28]. In [27], however, our conditions for factorability implicitly assume that the SPDC light is spatially filtered in such a way that only a single direction of propagation may reach the detectors. It can be shown that in most cases, the presence of even a small range of directions of propagation allowed to reach the detectors can reduce or even suppress the attainable factorability [28]. In this paper, we explain this behavior as resulting from photon pair correlations involving the spatial degree of freedom. Additionally, we identify a new expanded set of conditions for full spatio-temporal factorability that takes into account a realistic detection arrangement, such as coupling into single-mode fibers. We present results that show that the fulfillment of this expanded set of conditions indeed leads to photon pairs that approach full spatio-temporal factorability.

We compare two possible routes to bright, factorable and fiber-coupled photon-pair sources. On the one hand, we consider the above-described source, engineered for the suppression of most spatio-temporal correlations. For typical crystals, the requisite vector group velocity matching leads to the need for large signal/idler propagation angles. On the other hand, we also consider sources which have not been engineered for the suppression of spatio-temporal correlations and which involve typical values (smaller with respect to the engineered source) for the signal/idler propagation angles. For this second category of source, however, we allow the pump beam to be tightly focused at the crystal, and we likewise optimize the fiber-collection modes so as to maximize the resulting overlap with the generated modes. In order to eliminate spectral correlations between the fiber-coupled signal and idler modes, we also allow the use of spectral filters for the second category of source. Spatial correlations that tend to be enhanced at larger angles of emission are mostly suppressed for the engineered source; however, those spatial correlations that remain imply that the overlap of the emitted modes and the fiber-collection modes is reduced with respect to the ideal case of full spatio-temporal factorability. We present numerical simulations that indicate that the net effect is that the two categories of source considered lead to a brightness of the same order of magnitude and drastically higher than for an unengineered source.

2. The two-photon state and factorability

We consider for the present analysis a type-I, non-collinear source of SPDC photon pairs. We model the broadband pump beam as a chromatic superposition of single-frequency Gaussian beams, with a coincident beamwaist of radius w_0 and a coincident central direction of

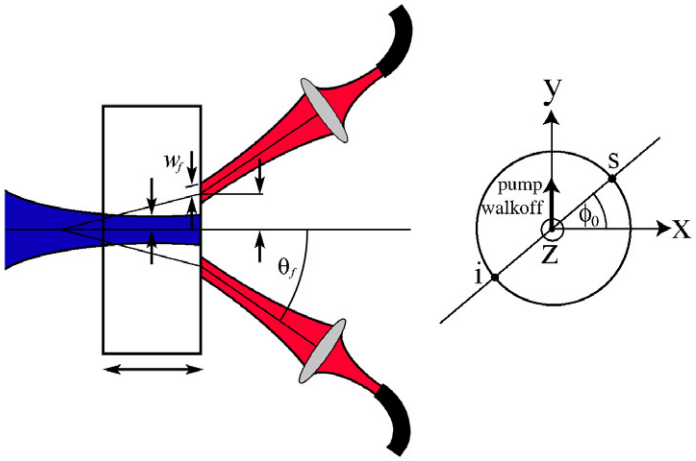

Figure 1. (a) Schematic diagram of the photon-pair source, showing the nonlinear crystal, pumped by a Gaussian beam. The refracted signal and idler modes are coupled into separate optical fibers. (b) Transverse section of the source, looking at the pump beam. The pump walk-off and central directions of propagation for collected signal and idler modes are indicated.

propagation. We assume a spectral weighting factor for the pump given by a Gaussian function with bandwidth σ and central frequency $\omega_{\mathrm{p}0}$. Likewise, we assume that the crystal has transverse dimensions much larger than the pump beam waist and that the crystal effective nonlinearity d is constant within the crystal. The signal and idler modes are assumed to be coupled into separate single-mode fibers. Fiber-collection modes are described by Gaussian beams, with their beam waists at the output face of the nonlinear crystal. Figure 1(a) presents a schematic of the source, where we have indicated some of the defining parameters: crystal length L, pump Gaussian beam radius at the beam waist w_0, angle of orientation of the fiber-collection modes θ_{f} (chosen so as to maximize the overlap between the fiber-collection modes and the signal and idler modes, refracted from the crystal into free space), fiber-collection mode radius at the beam waist w_{f} and fiber-collection mode height h on the crystal's output face. We take into account the existence of transverse spatial walk-off for the pump beam (for a negative uniaxial crystal, the generated photons are ordinary rays and therefore do not exhibit spatial walk-off). The coordinate system to be used is chosen so that the z-axis is parallel to the pump beam and the y-axis is parallel to the projection of the pump walk-off direction along the transverse plane (see figure 1(b)). ϕ_0 indicates the azimuthal orientation of the detection plane formed by the central directions of propagation of the two fiber-collection modes.

2.1. The two-photon quantum state

The electric field amplitude associated with the pulsed pump beam is described classically as a superposition of single-frequency Gaussian beams as follows:

$$E_{\mathrm{p}}(\vec{r},t) = (2\pi)^3 A_{\mathrm{p}} \int \mathrm{d}\omega_{\mathrm{p}}\, \alpha(\omega_{\mathrm{p}})\, \mathrm{e}^{\mathrm{i}(k_{\mathrm{p}}(\omega_{\mathrm{p}})z-\omega_{\mathrm{p}}t)} \mathrm{GB}(x,\, y+(z+L)\tan\rho_0,\, z-z_0+\tfrac{1}{2}L;\, \omega_{\mathrm{p}}) \qquad (1)$$

in terms of the Gaussian-beam spatial distribution $A_{\rm p}{\rm GB}(\vec{r};\omega)$, and the pump spectral amplitude $\alpha(\omega)$, assumed to be well described by a Gaussian function, centered at $\omega_{\rm p0}$ with width σ

$$\alpha(\omega) = \exp\left[-\frac{(\omega-\omega_{\rm p0})^2}{\sigma^2}\right]. \tag{2}$$

The Poynting vector walk-off of the pump beam, quantified by the walk-off angle ρ_0, is assumed to be parallel to the z–y-plane. The coefficient $A_{\rm p}$, with units of electric field per second, is related to the energy per pulse $U_{\rm p}$; for a weakly focused Gaussian beam, it is given according to the following formula:

$$A_{\rm p}^2 = \frac{2\sqrt{2}U_{\rm p}}{\pi\sqrt{\pi}(2\pi)^7 c\epsilon_0\sigma w_0^2}. \tag{3}$$

We have assumed that the beamwaist for the Gaussian beam associated with each pump spectral component is located at position $z = z_0$, measured with respect to the crystal middle plane. Here, the function ${\rm GB}(\vec{r};\omega)$ represents the paraxial Gaussian beam electric field amplitude,

$${\rm GB}(x,y,z;\omega) = \frac{1}{1+{\rm i}\frac{z}{z_{\rm R}}}\exp\left[-\frac{x^2+y^2}{w_0^2\left(1+{\rm i}\frac{z}{z_{\rm R}}\right)}\right], \tag{4}$$

where $z_{\rm R}$ is the Rayleigh range, expressed in terms of the radius at the beamwaist w_0, as $z_{\rm R} = k_{\rm p}w_0^2/2$. Note that while the function ${\rm GB}(x,y,z;\omega)$ can exhibit frequency dependence (through parameters w_0 and $z_{\rm R}$), in this paper we approximate this function to be frequency independent (this approximation is well justified for typical pump bandwidths), evaluating it at the central pump frequency. Following a standard perturbative approach, the quantum state produced by spontaneous SPDC may then be expressed as

$$|\Psi\rangle = |{\rm vac}\rangle + \eta\int {\rm d}\vec{k}_{\rm s}\int {\rm d}\vec{k}_{\rm i}\, F(\vec{k}_{\rm s},\vec{k}_{\rm i})\,\hat{a}_{\rm s}^{\dagger}(\vec{k}_{\rm s})\hat{a}_{\rm i}^{\dagger}(\vec{k}_{\rm i})|{\rm vac}\rangle. \tag{5}$$

Here, $F(\vec{k}_{\rm s},\vec{k}_{\rm i})$ represents the two-photon wavevector joint amplitude, and η is a constant given by $\eta = (4\pi^2\epsilon_0/\hbar)dLw_0^2A_{\rm p}$. The joint amplitude can in turn be expressed as

$$F(\vec{k}_{\rm s},\vec{k}_{\rm i}) = \ell(\vec{k}_{\rm s})\ell(\vec{k}_{\rm i})\alpha(\omega_{\rm s}+\omega_{\rm i})\phi(\vec{k}_{\rm s},\vec{k}_{\rm i}), \tag{6}$$

in terms of the function $\ell(\vec{k}) = [\hbar\omega/(\epsilon_0 n(\vec{k})^2)]^{1/2}$ and the phasematching function

$$\phi(\vec{k}_{\rm s},\vec{k}_{\rm i}) = \exp\left({\rm i}\frac{|\underline{k}_{\perp}|^2}{2k_{\rm p}}z_0\right)\exp\left[{\rm i}\tfrac{1}{2}L(\Delta k+\underline{k}_{\perp y}\tan\rho_0)\right]\exp\left(-\tfrac{1}{4}w_0^2|\underline{k}_{\perp}|^2\right){\rm sinc}\left(\tfrac{1}{2}L\Delta k\right). \tag{7}$$

Here, we have made the following definitions (an underlined symbol indicates a two-dimensional transverse vector) in terms of the Cartesian components of the signal and idler wavevectors:

$$\underline{k}_{\perp} \equiv (k_{{\rm s}x}+k_{{\rm i}x}, k_{{\rm s}y}+k_{{\rm i}y}), \tag{8}$$

$$\Delta k \equiv k_{\rm p} - \frac{|\underline{k}_{\perp}|^2}{2k_{\rm p}} - k_{{\rm s}z} - k_{{\rm i}z} + \underline{k}_{\perp y}\tan\rho_0. \tag{9}$$

Note that the wavevectors in the two-photon state above refer to internal wavevectors in the crystal; refraction into free space is taken into account below, in the context of fiber coupling of

the signal and idler photon pairs. The crystal cut orientation is selected so that the signal photon is centered at a frequency ω_{s0}, with this frequency component emitted in a direction given by polar angle $\theta_s = \theta_{s0}$; likewise, the selected crystal cut orientation is assumed to be such that the central emission frequency for the idler photon is $\omega_i = \omega_p - \omega_{s0} = \omega_{i0}$, with this frequency component emitted at polar angle $\theta_i = \theta_{i0}$.

2.2. Photon pair factorability and single-photon purity

While in the process of SPDC, photon pair emission occurs at random times, quantum information processing protocols require ideally on-demand generation of single photons, or at least emission of single photons at verifiable times. One way to counteract the characteristic randomness of SPDC photon pair emission is to detect one of the two photons so as to herald the existence of the conjugate photon. However, measuring part of an entangled state—in this case one of the two photons—leaves the remaining part—in this case the other photon—in a quantum-mechanically mixed state. Mathematically, tracing over one part of a quantum state leaves the remaining part in a statistical mixture of the allowed modes. This is an important limitation, because highly quantum-mechanically mixed single photons cannot interfere with other single photons, a key requirement for the implementation of quantum information processing protocols.

The single-photon mixedness referred to above occurs in the degrees of freedom available to the photons and in which photon-pair entanglement resides. Nonlinear optical sources may be entangled in a number of degrees of freedom including polarization, frequency and transverse momentum, which leads to the need for careful source design in order to avoid heralded single-photon mixedness. Note that it is straightforward to design SPDC photon pair sources that are unentangled in polarization, a design characteristic of all sources considered in this paper. In addition, we are particularly interested in fiber-coupled photon pair sources, where each of the two single-photons is coupled into a single-mode fiber, leading to the projection of the quantum state into specific transverse modes. While this projection necessarily suppresses entanglement in the transverse momentum degree of freedom, it can lead to an important reduction in source brightness if the generation and fiber-collection modes are not well matched to each other. As will be discussed below, this means that it is crucial to engineer the source so that photon pairs exhibit the best possible overlap with the fiber-collection modes and thus optimize the fiber-collection efficiency and the resulting source brightness.

Following from the above arguments, for the type of source of interest in this paper, frequency represents the only remaining degree of freedom where entanglement may reside. One way to suppress the resulting spectral (temporal) mixedness in the heralded single photon is to spectrally or temporally filter the herald photon, at the expense of the heralded photon flux. Another possibility is to spectrally or temporally filter the heralded photon, at the expense of an increased vacuum contribution, i.e. of a reduced heralding efficiency. In this paper, we explore experimental techniques that may be used for attaining photon pair factorability, based on two different strategies: (i) engineering photon pair sources in order to suppress entanglement at the source and (ii) the use of spectral filtering.

In general, the quantum state of the downconverted photons is said to be separable, or factorable, if $F(\vec{k}_s, \vec{k}_i) = S(\vec{k}_s)I(\vec{k}_i)$, i.e. if the two-photon wavevector joint amplitude can be written as the product of two functions, $S(\vec{k}_s)$ and $I(\vec{k}_i)$, each one a function that depends solely on the variables of one of the two photons. Formally, the degree of factorability can be

quantified by the inverse Schmidt number K^{-1} [26] or alternatively the degree of entanglement can be quantified by the Schmidt number K (where $K \to \infty$ denotes a maximally entangled state and $K = 1$ denotes a perfect factorable state). The purity can be quantified as $\mathrm{Tr}(\hat{\rho}_s^{\,2})$, where $\hat{\rho}_s = \mathrm{Tr}_i(|\Psi\rangle\langle\Psi|)$ represents the density operator for the heralded single photon in the signal mode and where Tr_i represents a partial trace over the idler mode. The relationship obeyed between K and $\mathrm{Tr}(\hat{\rho}_s^{\,2})$ is $\mathrm{Tr}(\hat{\rho}_s^{\,2}) = K^{-1}$, so that perfect heralded single-photon purity requires a factorable two-photon state [2]. Also, note that a monochromatic pump at ω_p leads to a one-to-one relationship between the signal-mode frequency ω_s and the corresponding idler frequency $\omega_p - \omega_s$ and therefore to maximal spectral entanglement; according to the above argument, this in turn leads to a highly mixed heralded single photon. Because we are interested in the generation of pure heralded single photons, the search for the experimental conditions under which we might generate fiber-coupled, factorable signal and idler photon pairs, while maintaining the largest possible brightness, is the key motivation behind this paper.

2.3. Conditions for factorability of the two-photon state

We can write the wavevectors in terms of their Cartesian components expressed in spherical coordinates, i.e. $\vec{k}_\mu = [n(\omega_\mu)\omega_\mu/c]\hat{k}_\mu(\theta_\mu, \phi_\mu)$, where

$$\hat{k}_\mu(\theta_\mu, \phi_\mu) = (\sin\theta_\mu \cos\phi_\mu, \sin\theta_\mu \sin\phi_\mu, \cos\theta_\mu). \tag{10}$$

We also define wavevectors $\vec{k}_{\mu 0}$ (with $\mu = s, i$) as the wavevectors corresponding to the central values $\omega_{\mu 0}$, $\theta_{\mu 0}$, and $\phi_{\mu 0}$. In this manner, the wavevector joint amplitude may be expressed as a function of six variables, corresponding to the frequency ω_μ, polar angle θ_μ and azimuthal angle ϕ_μ, for each of the two photons ($\mu = s, i$),

$$F(\vec{k}_s, \vec{k}_i) \to F(\omega_s, \theta_s, \phi_s; \omega_i, \theta_i, \phi_i). \tag{11}$$

The problem of finding an optimum region in parameter space for generating factorable photon pairs turns out to be difficult, since the wavevector joint amplitude given by equation (6) depends on six variables and on a large number of parameters. It has been shown theoretically and experimentally that the expansion to first order in transverse wavenumber and frequency of the joint amplitude function, and the substitution of the sinc function in equation (6) with an appropriately chosen Gaussian function, yields a description of the two-photon state that in some respects is sufficiently accurate, even for SPDC configurations with Poynting-vector walk-off [29, 30]. The advantage of these approximations is that it becomes straightforward to carry out further analytic calculations. In particular, it becomes possible to derive the conditions for factorability of the two-photon state. Note that while we use the conditions for factorability as a guide for the selection of experimental parameters, our numerical calculations shown below are based on the full two-photon state, without resorting to approximations.

We will proceed as follows. As a first step, we will derive general conditions that ensure factorability of the photon pairs under the approximations described in the previous paragraph. As a second step, these conditions will be used for obtaining a specific source design, i.e. specific values for all relevant source parameters, predicted (by the conditions derived in step 1) to yield factorable photon pairs. As a third step, we will verify numerically that the source design obtained in step 2 indeed yields photon pairs that approach full spatio-temporal factorability. Note that for this third step, we rely on the full two-photon state, without resorting to approximations.

Specifically, in order to write the joint amplitude entirely in terms of exponential functions, we use the approximation $\mathrm{sinc}(x) \approx \exp(-\gamma x^2)$, with $\gamma \approx 0.193$ selected so that the two functions have an identical full-width at half-maximum. Next, we write the argument of the resulting Gaussian function as a first-order Taylor series in the six variables $\{\omega_s, \theta_s, \phi_s, \omega_i, \theta_i, \phi_i\}$, around the central values for each of these variables. Thus, in writing the argument of the joint wavevector amplitude, expressed fully in terms of an exponential function, as a power series of the six variables around the corresponding central values, any mixed terms between a variable of one photon and a variable corresponding to the other photon indicate the presence of entanglement between the signal and idler modes.

The analysis for a general plane of detection characterized by angle ϕ_0 leads to complicated expressions. In the appendix, we present the specific case of $\phi_0 = 0$, on which the factorability analysis below is based. We have found that for the crystal lengths considered here (e.g. $L = 300\,\mu$m) the effect of walk-off on the resulting two-photon state is negligible.

The resulting expression for the wavevector joint amplitude is expressed in terms of the variables $\Omega_\mu \equiv \omega_\mu - \omega_{\mu 0}$, $\Theta_\mu \equiv \theta_\mu - \theta_{\mu 0}$ and $\Phi_\mu \equiv \phi_\mu - \phi_{\mu 0}$. The factorability conditions arise from imposing a vanishing coefficient for each mixed term of the form $A_s B_i$ (or $A_i B_s$), with $A, B = \Omega, \Theta$. These conditions are as follows:

$$\text{Condition 1:} \quad k'_s = k'_p \cos\theta_{s0}, \tag{12}$$

$$\text{Condition 2:} \quad k'_i = k'_p \cos\theta_{i0}, \tag{13}$$

$$\text{Condition 3:} \quad \frac{w_0^2}{\gamma L^2} = -\tan\theta_{s0}\tan\theta_{i0}, \tag{14}$$

$$\text{Condition 4:} \quad \sigma_p \gtrsim \overline{\sigma}, \tag{15}$$

where $\overline{\sigma}$ represents a threshold bandwidth, which if exceeded implies that the joint amplitude of the two-photon state is determined by the longitudinal and transverse phasematching properties, independently of the pump bandwidth. In those cases where the signal and idler photons are each projected to a specific single spatial mode (e.g. fiber-collection modes), the two-photon state becomes a function only of the frequencies ω_s and ω_i. Under these circumstances, we may calculate the threshold bandwidth $\overline{\sigma}$ as the full-width at half-maximum of the function $\int \mathrm{d}\omega_- |f(\omega_+, \omega_-)|^2$, where the function f represents the joint amplitude projected to specific spatial modes, in the limit of infinite pump bandwidth, expressed in terms of the variables $\omega_\pm = \omega_s \pm \omega_i$.

Note that correlations involving the azimuthal angle variables Φ_μ cannot be made to vanish. However, they may be limited by reducing the detection angular spread. Indeed, if the following condition, shown for frequency degenerate SPDC where $k = |\vec{k}_s| = |\vec{k}_i|$ and $\theta_0 = \theta_{s0} = \theta_{i0}$, is also fulfilled,

$$\text{Condition 5:} \quad \Phi_{\max}^2(\gamma\rho^2 L^2 + w_0^2) \lesssim \frac{1}{k^2 \sin^2\theta_0}, \tag{16}$$

where $\Phi_{\max}$ represents the maximum spread of azimuthal angles around the central directions of signal and idler propagation, then correlations involving the azimuthal angle variables become negligible. Of course, in addition to conditions 1–5, phasematching must be observed, i.e. $\Delta k = 0$ (see equation (9)) for the central generation frequencies and directions of propagation.

Conditions 1 and 2 refer to vector group velocity matching: specifically, the longitudinal component of the signal and idler group velocities is made equal to the pump group velocity.

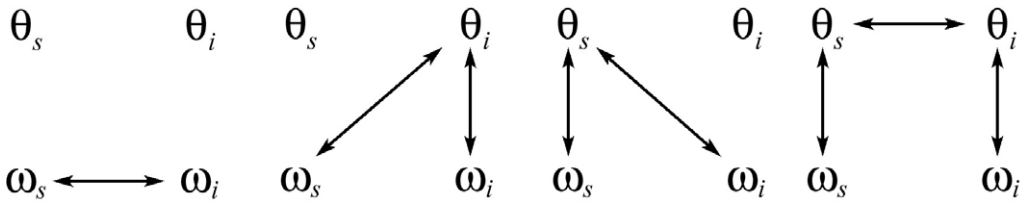

Figure 2. Effective spectral correlation diagrams for type-I non-collinear SPDC. Here, part (a) shows direct spectral correlations and parts (b)–(d) show indirect spectral correlations involving the polar angle variables. Omitted from this figure are effective spectral correlations involving azimuthal angle variables.

Of course, in the case of frequency-degenerate SPDC, these two conditions become a single condition. Condition 3 refers to a constraint on the physical dimensions of the source (crystal length and pump beam radius at the beamwaist), together with the angles of propagation. In common with other techniques for factorable photon-pair generation, the present technique requires a broadband pump, with a bandwidth exceeding the threshold presented in condition 4.

The joint intensity $|F(\omega_s, \theta_s, \phi_s; \omega_i, \theta_i, \phi_i)|^2$ may exhibit correlations between any two of its six arguments. We refer to correlations between variables corresponding to different photons, which of course contribute to photon-pair entanglement, as 'external' correlations. Likewise, we refer to correlations between two variables corresponding to the same photon, which do no not contribute to entanglement, as 'internal' correlations. A photon-pair source can, in general, be described by a joint amplitude that includes all of the above correlations.

In previous work, we have derived conditions for the suppression of spectral correlations in non-collinear type-I spontaneous PDC [27, 28]. However, in that work we did not consider the effect of correlations involving spatial variables (angles θ_μ and ϕ_μ in equation (10)) on the *effective* spectral correlations for a given detection arrangement. Assuming that correlations between azimuthal angle variables and polar angle/spectral variables can be neglected (these tend to be weak), figure 2 shows the possible scenarios that may result in the appearance of effective signal–idler spectral correlations. Figure 2(a) shows *direct* spectral correlations, which can be made to vanish if the conditions derived in [27] are fulfilled. However, as shown schematically in figures 2(b)–(d), effective correlations may arise in the following two scenarios: (i) the existence of internal ω–θ correlations, in conjunction with external θ–θ correlations, and (ii) the existence of external ω–θ correlations in conjunction with internal ω–θ correlations [39]. Such effective spectral correlations require a spread of detection wavevectors, i.e. a range of θ and ϕ values. One way to suppress these correlations is by restricting the spread of detection k-vectors through spatial filtering. A superior solution, which does not lead to a reduction of brightness, is the suppression of correlations involving spatial (angular) variables *at the source*. In this paper, we have derived conditions that result in the suppression of external correlations in all photonic degrees of freedom. For a source that fulfills these conditions, the spread of detection k-vectors may be increased without the appearance of effective spectral correlations.

As an illustration, let us consider a β-barium borate (BBO) crystal pumped by a train of ultrashort pulses centered at 405 nm, generating frequency-degenerate SPDC photon pairs, centered at 810 nm. The internal angle of emission at which vector group velocity matching occurs (computed from conditions 1 and 2 above) can be verified to be $\theta_{s0} = -\theta_{i0} = 9.96^\circ$. Note

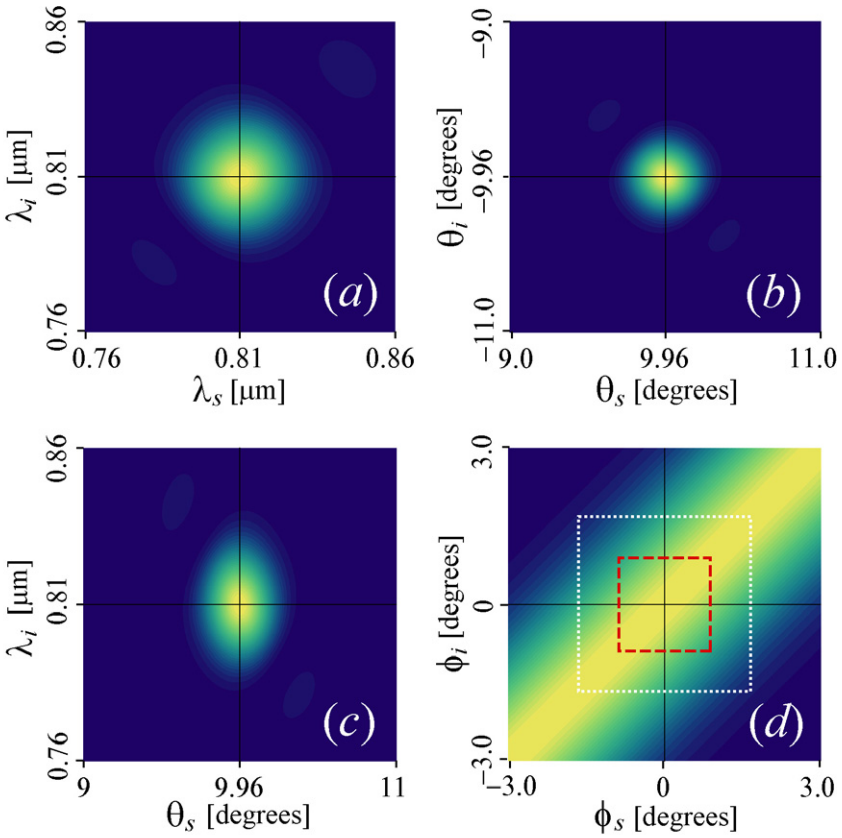

Figure 3. Plots of the joint intensity, $|F(\omega_s, \theta_s, \phi_s; \omega_i, \theta_i, \phi_i)|^2$, where four of the six variables are made constant, versus the remaining two. These plots show external correlations between the following pairs of variables: (a) generated frequencies (λ_s–λ_i), (b) polar angles (θ_s–θ_i), (c) wave length and polar angle (θ_s–ω_i) and (d) azimuthal angles (ϕ_s–ϕ_i). Azimuthal correlations can be suppressed by limiting $|\Phi_s|$ and $|\Phi_i|$ to values $\leqslant 1$ degrees as shown by the inner red-dashed-line square. The outer white-dotted-line square refers to the azimuthal-angle fiber acceptance, as discussed below in section 3.

that while this is a large angle of emission that leads to some difficulties (as will be discussed below), other typical crystals including BIBO, PPKTP and PPLN lead to even larger vector group velocity matching angles. For this angle of emission, and for the selected central emission frequency, the required crystal cut angle required to attain phasematching is $\theta_{pm} = 40.7^\circ$ (we also assume that the crystal is oriented such that the pump and the crystal axis have a relative azimuthal orientation of 30°, so that the effective nonlinearity can attain its maximum value). Assuming a crystal length of $L = 300\,\mu$m (we will present below a criterion for choosing the crystal length), condition 3 then results in a required pump beam radius of $w_0 = 23.2\,\mu$m. The fulfillment of conditions 1–4 results in a two-photon state, which is essentially factorable in the spectral and polar angle degrees of freedom. The pump bandwidth is selected so that condition 5 is fulfilled (this will be discussed in greater detail in section 3).

This factorability may be appreciated in figure 3, where we present plots of correlations between particular pairs of variables for the signal and idler photons. In each panel, four

of the six variables in the joint intensity $|F(\omega_s, \theta_s, \phi_s; \omega_i, \theta_i, \phi_i)|^2$ are made equal to their central values, while plotting versus the remaining two variables. Figure 3(a) shows spectral ω_s–ω_i correlations; figure 3(b) shows polar angle θ_s–θ_i correlations; figure 3(c) shows mixed spectral–spatial ω_i–θ_s correlations; figure 3(d) shows azimuthal angle ϕ_s–ϕ_i correlations. Note that while our analysis that results in the conditions for factorability (equation (A.13)) relies on the Gaussian approximation of the phasematching function and on a power series expansion, the plots in figure 3 were computed without any approximations.

As expected from the fulfillment of conditions 1–4, spectral, polar angle and mixed spectral–polar angle correlations are essentially suppressed. Azimuthal correlations cannot be made to vanish; however, by restricting the directions of propagation that are allowed to reach the detectors, these correlations may be essentially suppressed. This is illustrated by the red dashed line in figure 3(d), which corresponds to limiting azimuthal angles to $|\Phi_s|, |\Phi_i| \leqslant 1$ degrees. Note that mixed spectral–polar angle correlations ω_i–θ_s are similar to those shown in figure 3(c). Correlations between azimuthal angle variables and polar angle/frequency (not shown) are, for this particular source, essentially negligible.

2.4. Fiber-coupled two-photon state and flux

We are interested in studying the spectral properties of photon pairs coupled into separate single-mode fibers for the signal and idler modes (see figure 1(a)). To this end, it is instructive to consider the modes that would result from light exiting the fibers into free space through coupling lenses, and propagating backwards towards the crystal. According to our analysis below, and in agreement with intuition, the joint amplitude for the fiber-coupled photon pairs is given by the mathematical overlap between the fiber-collection modes in free space and the pre-fiber-coupling joint amplitude (see equation (24)) [31]–[33]. In this paper, we model the fiber-collection modes as Gaussian beams. Of course, the position and orientation of the fiber-collection modes must be selected to match the position and orientation of the signal and idler modes, refracted from the crystal into free space. Note that for SPDC photons propagating in a single-transverse mode environment, entanglement involving the spatial degrees of freedom is suppressed, leaving frequency as the only continuous-variable degree of freedom where entanglement may reside. As will become clear below, while spatial and mixed spectral-spatial entanglement cannot survive fiber-coupling, the degree of overlap between emission and fiber-collection modes can limit the resulting source brightness.

It is convenient to introduce single-photon states $|\omega\rangle_{F\mu}$ (with $\mu = s, i$) defined in terms of a specific superposition of plane waves, corresponding to the fiber collection modes

$$|\omega\rangle_{F\mu} = \hat{b}^\dagger_\mu(\omega)|\text{vac}\rangle, \tag{17}$$

where the annihilation operator $\hat{b}_\mu(\omega)$ is defined in terms of the weighting factor $\tilde{u}_\mu(\vec{k})$

$$\hat{b}_\mu(\omega) = \int_{|\vec{k}|=\omega/c} \mathrm{d}^2k\, \tilde{u}_\mu(\vec{k})\hat{a}_\mu(\vec{k}), \tag{18}$$

and the integral is carried out over all wavevectors with magnitude ω/c. Imposing the standard commutation relationship between $\hat{b}_\mu(\omega)$ and $\hat{b}^\dagger_\mu(\omega)$ leads to the following normalization constraint:

$$\int_{|\vec{k}|=\omega/c} \mathrm{d}^2k\, |\tilde{u}_\mu(\vec{k})|^2 = 1. \tag{19}$$

In the specific case where the fiber collection modes can be adequately described as Gaussian beams [31]–[33], the weighting factors $\tilde{u}_\mu(\vec{k})$ may be written as

$$\tilde{u}_\mu(\vec{k}) = \tilde{u}_0(\omega, \theta_0)\ \exp\left(-\tfrac{1}{4}w^2[\sec^2\theta_0(k_x - k_\mu \sin\theta_0)^2 + k_y^2]\right)\ \mathrm{e}^{\mathrm{i}hk_x}, \tag{20}$$

where we have neglected certain terms associated with diffraction of the fiber-collection modes and where we have assumed that the fiber-collection modes are centered at $\phi_0 = 0$. Here, the Gaussian-beam electric field spatial distribution is tilted at an angle θ_0, laterally shifted by distance h and evaluated on the second face of the crystal. The function $\tilde{u}_0(\omega, \theta_0)$ represents a normalization coefficient.

The fiber-coupled two-photon state $|\Psi\rangle_c$ can then be written as

$$|\Psi\rangle_c = \hat{\Pi}|\Psi\rangle \tag{21}$$

in terms of the projection operator $\hat{\Pi}$ defined as

$$\hat{\Pi} = \frac{1}{c^2}\int \mathrm{d}\omega_\mathrm{s}\, |\omega_\mathrm{s}\rangle_{\mathrm{Fs}}\langle\omega_\mathrm{s}|_{\mathrm{Fs}} \otimes \int \mathrm{d}\omega_\mathrm{i}\, |\omega_\mathrm{i}\rangle_{\mathrm{Fi}}\langle\omega_\mathrm{i}|_{\mathrm{Fi}}. \tag{22}$$

By substituting equations (5) and (22) into equation (21), we can write the fiber-coupled two-photon state as

$$|\Psi\rangle_c = |\mathrm{vac}\rangle + \frac{\eta}{c^2}\int \mathrm{d}\omega_\mathrm{s} \int \mathrm{d}\omega_\mathrm{i}\, f(\omega_\mathrm{s}, \omega_\mathrm{i})\, |\omega_\mathrm{s}\rangle_{\mathrm{Fs}}|\omega_\mathrm{i}\rangle_{\mathrm{Fi}}, \tag{23}$$

where the resulting fiber-coupled joint spectral amplitude $f(\omega_\mathrm{s}, \omega_\mathrm{i})$ is calculated in terms of the fiber modes $\tilde{u}_\mu(\vec{k}_\mu)$ and the wavevector joint amplitude in free space $F_\mathbf{f}(\vec{k}_\mathrm{s}, \vec{k}_\mathrm{i})$ as

$$f(\omega_\mathrm{s}, \omega_\mathrm{i}) = \int_{|\vec{k}_\mathrm{s}|=\omega_\mathrm{s}/c} \mathrm{d}^2k_\mathrm{s} \int_{|\vec{k}_\mathrm{i}|=\omega_\mathrm{i}/c} \mathrm{d}^2k_\mathrm{i}\ F_\mathbf{f}(\vec{k}_\mathrm{s}, \vec{k}_\mathrm{i})\, \tilde{u}_\mathrm{s}^*(\vec{k}_\mathrm{s})\tilde{u}_\mathrm{i}^*(\vec{k}_\mathrm{i}). \tag{24}$$

Note that the free-space joint amplitude $F_\mathbf{f}(\vec{k}_\mathrm{s}, \vec{k}_\mathrm{i})$ is obtained from the intra-crystal joint amplitude $F(\vec{k}_\mathrm{s}, \vec{k}_\mathrm{i})$ by substituting each polar angle with its refracted version, i.e. $\theta_\mu \to \arcsin(\sin(\theta_\mu)/n(\vec{k}))$ with $\mu = \mathrm{s}, \mathrm{i}$. The number of photon pairs produced per pump pulse, and coupled into separate fibers for the signal and idler modes, can then be easily computed as

$$\begin{aligned} N &= \int \mathrm{d}\omega_\mathrm{s} \int \mathrm{d}\omega_\mathrm{i} \langle\Psi|_c\, \hat{b}_\mathrm{s}^\dagger(\omega_\mathrm{s})\hat{b}_\mathrm{i}^\dagger(\omega_\mathrm{i})\hat{b}_\mathrm{i}(\omega_\mathrm{i})\hat{b}_\mathrm{s}(\omega_\mathrm{s})\, |\Psi\rangle_c \\ &= \frac{\eta^2}{c^2}\int \mathrm{d}\omega_\mathrm{s} \int \mathrm{d}\omega_\mathrm{i}\, |f(\omega_\mathrm{s}, \omega_\mathrm{i})|^2. \end{aligned} \tag{25}$$

Another quantity of interest is the heralding efficiency, defined as N/N_s where N_s represents the signal-mode detection rate, which includes signal-mode detection events for which no corresponding idler photon is detected. The heralding efficiency represents the probability that a single photon is present in the idler-mode fiber, conditioned on the presence of a single photon in the signal-mode fiber [34]. It may be shown that N_s is given as follows:

$$N_\mathrm{s} = \frac{\eta^2}{c^2}\int \mathrm{d}\omega_\mathrm{s} \int \mathrm{d}\omega_\mathrm{i} \int_{|\vec{k}_\mathrm{i}|=\omega_\mathrm{i}/c} \mathrm{d}^2k_\mathrm{i} \left| \int_{|\vec{k}_\mathrm{s}|=\omega_\mathrm{s}/c} \mathrm{d}^2k_\mathrm{s}\tilde{u}_\mathrm{s}^*(\vec{k}_\mathrm{s})\, F_\mathbf{f}(\vec{k}_\mathrm{s}, \vec{k}_\mathrm{i}) \right|^2. \tag{26}$$

Note that it can be shown from equations (25) and (26) that in the strong spatial filtering limit where only a single k-vector for each of the signal and idler modes is retained, N/N_s can approach unity. This, however, has limited practical relevance, since strong spatial filtering is incompatible with an optimization of the source brightness.

We now develop an approximate expression for the brightness, which leads to greater physical insight. From equation (25) and for a sufficiently small emission bandwidth, we may write $N \approx \eta^2 \Delta\omega_s \Delta\omega_i |f(\omega_{s0}, \omega_{i0})|^2/c^2$ in terms of the signal-mode emission bandwidth $\Delta\omega_s$ and the idler-mode emission bandwidth $\Delta\omega_i$. This leads to the following approximate expression for the source brightness,

$$N \approx \frac{1}{2\sqrt{2}\pi^{\frac{9}{2}}\epsilon_0 c^7} \omega_0^6 d^2 U_p L^2 w_0^2 \frac{\Delta\omega_s \Delta\omega_i}{\sigma} \mathscr{S}_0 |\mathscr{O}_0|^2, \tag{27}$$

in terms of the following definitions, $\mathscr{S}_0 \equiv \mathscr{S}(\omega_{s0}, \omega_{i0})$ and $\mathscr{O}_0 \equiv \mathscr{O}(\omega_{s0}, \omega_{i0})$, with

$$\mathscr{S}(\omega_s, \omega_i) \equiv \int_{\mathscr{C}_s} d^2k_s \int_{\mathscr{C}_i} d^2k_i |\hat{F}(\vec{k}_s, \vec{k}_i)|^2, \tag{28}$$

$$\mathscr{O}(\omega_s, \omega_i) \equiv \int_{\mathscr{C}_s} d^2k_s \int_{\mathscr{C}_i} d^2k_i \, \mathscr{F}(\vec{k}_s, \vec{k}_i) \, \tilde{u}_s^*(\vec{k}_s) \tilde{u}_i^*(\vec{k}_i). \tag{29}$$

In the above two equations, $\mathscr{C}_\mu$ (with $\mu = s, i$) represents an area of transverse wavevector space, defined by the fiber acceptance. Also, we have defined $\hat{F}(\vec{k}_s, \vec{k}_i) \equiv F(\vec{k}_s, \vec{k}_i)/F(\vec{k}_{s0}, \vec{k}_{i0})$ and $\mathscr{F}(\vec{k}_s, \vec{k}_i)$ represents the joint wavevector amplitude, normalized so that

$$\int_{\mathscr{C}_s} d^2k_s \int_{\mathscr{C}_i} d^2k_i |\mathscr{F}(\vec{k}_s, \vec{k}_i)|^2 = 1. \tag{30}$$

The quantity $|\mathscr{O}(\omega_s, \omega_i)|^2$ is constrained to take values $0 \leqslant |\mathscr{O}(\omega_s, \omega_i)|^2 \leqslant 1$ and represents the degree of overlap between the SPDC emission mode and the fiber collection modes; while a value of 0 indicates no overlap, a value of 1 indicates perfect overlap. Note that because $\mathscr{O}(\omega_s, \omega_i)$ is dependent on $\mathscr{C}_s$ and $\mathscr{C}_i$, in order to meaningfully compare different sources in terms of their respective degrees of overlap, a consistent definition of $\mathscr{C}_s$ and $\mathscr{C}_i$ should be used. Note that $|\mathscr{O}(\omega_s, \omega_i)|^2 = 1$ implies that the emission mode is identical to the fiber-collection modes; since the function $\tilde{u}(\vec{k}_s)\tilde{u}(\vec{k}_i)$ is factorable, this means that the photon-pair state must be engineered to be factorable in order to ensure the highest possible rate of photon-pair fiber coupling. $\mathscr{S}(\omega_s, \omega_i)$ is related to the extent, in transverse signal and idler wavevector space, of the emitted state. More precisely, this quantity represents the (frequency-dependent) extent, in transverse signal and idler wavevector space, of an equivalent rectangular function (in place of $|\hat{F}(\vec{k}_s, \vec{k}_i)|^2$) with the same value of the integral which defines $\mathscr{S}(\omega_s, \omega_i)$. Note that in cases where the function $\hat{F}(\vec{k}_s, \vec{k}_i)$ is factorable, i.e. where $\hat{F}(\vec{k}_s, \vec{k}_i) = S(\vec{k}_s) I(\vec{k}_i)$, this becomes

$$\mathscr{S} = \int d\theta_s \int d\phi_s \sin\theta_s |S(\vec{k}_s)|^2 \int d\theta_i \int d\phi_i \sin\theta_i |I(\vec{k}_s)|^2 = \Omega_s \Omega_i. \tag{31}$$

Here, $\Omega_s \equiv \int d\theta_s \int d\phi_s \sin\theta_s |S(\vec{k}_s)|^2$ (and similarly for the idler photon) may be interpreted as an effective emission solid angle. Note that equation (27) is consistent with intuition: the source brightness is proportional to the emission bandwidth, to the source transverse wavevector extent and to the degree of overlap between the emission and fiber-collection modes. Note that if we increase the emission bandwidth by a factor a, in general we also need to increase the pump bandwidth by a factor a to maintain factorability. This makes the factor $(\Delta\omega_s \Delta\omega_i)/\sigma$ (and therefore the source brightness while imposing factorability) linear in the SPDC emission bandwidth.

We see from this that the brightness per mode (spectral and spatial) and per unit pump-pulse energy $N_m \equiv N/(\Delta\omega_s \Delta\omega_i \mathscr{S} U_p)$ for two sources centered at the same frequency, involving

crystals of the same length, and pump beams with identical radii, depends on d^2 (over which we have no control for a given choice of crystal), on σ that is tied to the emission bandwidth to guarantee factorability and therefore cannot be changed freely and on the degree of overlap $|\mathscr{O}|^2$. Thus, N_{m} is controlled basically by the degree of overlap, independently of the specific technique used for source optimization. Note that this limits the scope for brightness optimization for engineered versus unengineered sources.

3. Results and discussion

In order to compare the performance of various sources of interest, in this section we present the results of numerical simulations leading to values for the heralded single-photon purity and the source brightness. Note that while we use the factorability analysis resulting from the Gaussian and first-order approximations of section 2.3 as a guide for the selection of values for the various experimental parameters, all numerical simulations to be shown here are based on the full two-photon state, without resorting to approximations.

For all the sources considered here, we assume a pump centered at 405 nm, which can be obtained through second harmonic generation from a Ti:sapphire oscillator, with frequency-degenerate signal and idler photon pairs centered at 810 nm. We wish to compare the performance of the engineered source of section 2.3 with an unengineered source. In order to make this comparison as useful as possible, we assume the same type of crystal (i.e. BBO), the same crystal length ($L = 300\,\mu$m) and the same energy per pump pulse (6.25×10^{-9} J), which corresponds to a pump power of 500 mW at a repetition rate of 80 MHz, for both categories of sources. The engineered source relies on vector group velocity matching for the suppression of spatio-temporal entanglement. Such group velocity matching occurs for large signal/idler propagation angles (9.96°, internal, for the example in section 2.3). We also consider a source, to be referred to as unengineered, which involves propagation angles similar to those used in several recent experiments (see, for example, [35]) and which we consider as typical. Specifically, for this source we assume an internal propagation angle (i.e. prior to refraction at the crystal–air interface) of 2°. As its name suggests, for this source we make no effort to engineer the spatio-temporal properties of the photon pairs. Likewise, no effort is made to tailor the SPDC emission mode to the fiber-collection modes: we assume a weakly focused pump beam with a radius at the beamwaist of $w_0 = 1$ mm. The required crystal cut angle for this source is $\theta_{\mathrm{pm}} = 29.33°$, and we assume that the crystal is oriented so that the pump and the crystal axis have a relative azimuthal orientation of 30°.

For the unengineered source, we consider two additional variants: (i) an unengineered source for which the fiber-coupled signal and idler modes are spectrally filtered to render the photon pairs nearly factorable, and (ii) in addition to the presence of SPDC spectral filtering, the pump beam is focused to the same degree as for the engineered source, and the width of the fiber collection modes is optimized for maximum source brightness. We refer to the latter two sources as UF (for unengineered, filtered) and UFF (for unengineered, pump-focused, filtered).

For each source configuration, the pump bandwidth is selected as $\sigma = 2.0 \times \overline{\sigma}$, where $\overline{\sigma}$ refers to the bandwidth corresponding to the threshold value from our condition 4 above (see section 2.3). The factor of 2.0 ensures that the two-photon properties are defined by the phasematching properties, tailored for factorability, rather than by the pump bandwidth. Note that conditions 1–3 (see equations (12)–(14)) ensure factorability in the infinite pump bandwidth limit. Thus, a larger pump bandwidth (than $\overline{\sigma}$ defined in the context of condition 4) could lead

Table 1. This table shows the parameters (pump beam radius w_0, fiber-collection mode radius w_f, pump bandwidth σ and signal/idler filter bandwidth $\Delta\lambda$) that define each of the four sources considered: engineered, unengineered, UF and UFF. The value of the fiber-collection mode radius w_f shown corresponds to that which maximizes the brightness for each of the sources. Note that '–' indicates that no value applies.

Source	w_0 (μm)	w_f (μm)	σ (THz)	$\Delta\lambda$ (nm)
Engineered	23.1	21.5	142.2	–
Unengineered	1000	14.3	91.1	–
UF	1000	14.3	46.7	15.3
UFF	23.1	11.4	51.0	17.5

to a greater degree of factorability, although in practice this is limited by the available laser bandwidth. Also, increasing σ leads to a reduced flux, since the pump frequency components near the edges of the pump spectrum involve weaker phasematching and therefore a more limited contribution to the source brightness.

When describing the effect of fiber coupling on SPDC photon pairs, the degree of focusing of the fiber-collection modes plays a crucial role [36]. Indeed, we find that for a given pump beam radius w_0, the fiber-collection mode radius on the output face of the crystal w_f is of fundamental importance. Specifically, we find that there is a particular value of w_f that optimizes the resulting brightness for a given source configuration while not deteriorating the photon-pair separability. Such an optimum w_f characterizes the fiber-collection modes that lead to the best overlap with the SPDC light spatial distribution. This is clear from figures 4(a) and (b), which show the expected heralded single-photon purity and the source brightness as a function of w_f, for each of the four sources considered.

Table 1 summarizes the values of the experimental parameters that define the four sources considered: engineered, unengineered, UF and UFF.

In what follows we compare these four sources (engineered, typical, UF and UFF) in terms of the source brightness and the degree of factorability. In order to characterize each of the sources considered, we employ the heralded single-photon purity $\mathrm{Tr}(\hat{\rho}_s^{\,2})$ and the source brightness N (see section 2.4).

Figures 4(c)–(e) show the fiber-coupled joint spectra for three of the sources considered here (engineered, unengineered and UFF), where for each case we have selected the optimum fiber-collection mode radius. The engineered source leads to an optimum brightness of 0.20 fiber-coupled photon pairs per pump pulse, which occurs for $w_f = 21.6\,\mu$m, resulting in a purity of $\mathrm{Tr}(\hat{\rho}_2^2) = 0.96$, observed for a pump bandwidth of $\Delta\lambda_{\mathrm{pump}} = 2.0 \times \overline{\Delta\lambda} = 29.1$ nm. Because the resulting two-photon state is nearly factorable, weak spectral filtering would suffice to attain a nearly optimum single-photon purity. Note that although each of conditions 1–4 is fulfilled, condition 5 is not. Indeed, the fiber azimuthal angular acceptance (calculated at $1/e$) of $\Phi_{\mathrm{max}} = 3.4^\circ$ (shown by the outer white-dashed-line box in figure 3(d)) is such that azimuthal correlations are not altogether suppressed.

In contrast, the unengineered source leads to a comparatively low single-photon purity, which, in the vicinity of the maximum expected brightness, reaches values of ~ 0.2.

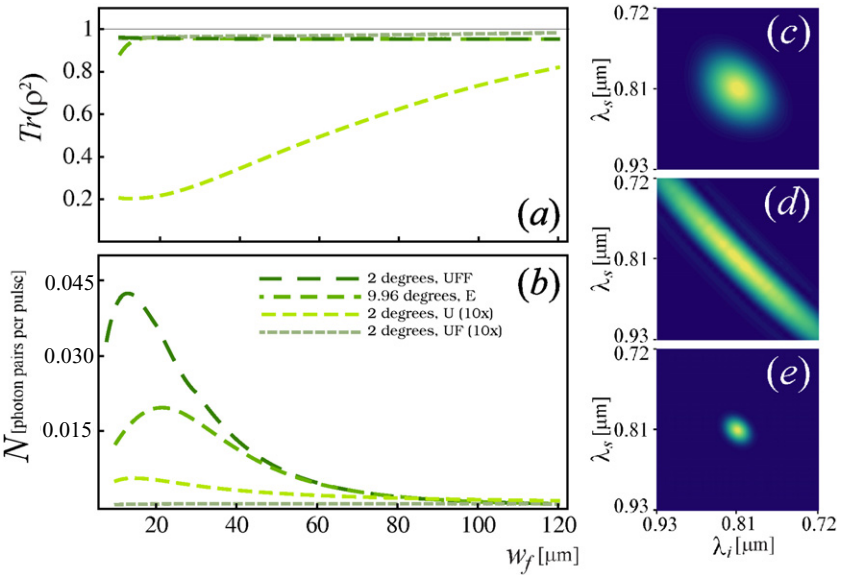

Figure 4. (a) Purity for the single heralded photon in the signal mode $\mathrm{Tr}(\rho_s^2)$, versus fiber collection mode radius w_f, for four sources of interest: (i) engineered source (E), (ii) unengineered source (U), (iii) unengineered, filtered (UF) source and (iv) unengineered, pump-focused, filtered (UFF) source. (b) Brightness (number of fiber-coupled photon pairs per pump pulse) as a function of w_f for the above four sources. (c–e) Coupled joint spectra $f(\omega_s, \omega_i)$, plotted for each of three of the sources (engineered, unengineered and UFF), in each case for the optimum value of w_f. In this figure, for each configuration the pump bandwidth σ has been taken as 2.0 times the corresponding threshold value $\overline{\sigma}$ related to condition 5 for factorability.

Figures 4(c) and (d) show the expected behavior: while the engineered source leads to a nearly factorable joint spectrum, the unengineered source exhibits strong spectral correlations. Of course, a possible strategy to impose factorability on the unengineered source is to spectrally filter the signal and idler photons with a sufficiently small bandwidth. However, this is achieved at the cost of a significant reduction of the two-photon flux. In figure 4(a) and (b), we show the single-photon purity and source brightness for the UF source, which corresponds to an unengineered source rendered factorable through Gaussian-profile spectral filters acting on the signal and idler modes. For the specific case considered here, a filter with a full transmission width at half-maximum of 15.3 nm (selected to reach the same single-photon purity as the engineered source) leads to a flux ~ 496 times greater in the case of the engineered source, compared to the unengineered source, as shown in figure 4(b).

Table 2 shows some of the factors appearing in equation (27) computed for each of the sources, divided by the corresponding values for each of the engineered source. Thus, a value smaller than unity implies that the engineered source outperforms the source in question, while a value greater than unity implies that the engineered source underperforms the source in question. Here, $\mathscr{C}_s$ and $\mathscr{C}_i$ (see equations (29) and (30)) are selected to include all transverse wavevectors with $|\tilde{u}(\vec{k}_s)\tilde{u}(\vec{k}_i)|^2$ values greater than or equal to $1/100$ of the maximum value. As may be seen from the table, when compared to the unengineered source, the engineered source leads to

Table 2. This table shows some of the factors that appear in equation (27), for each of the sources listed in the table, normalized by the corresponding value for the engineered source.

	$1/\sigma$	d^2	w_0^2	$\mathscr{S}$	$\lvert\mathscr{O}\rvert^2$	$\Delta\omega^2$
Engineered	1.0	1.0	1.0	1.0	1.0	1.0
Unengineered	1.56	1.39	1866.4	0.0037	0.0011	17.99
UF	3.03	1.39	1866.4	0.0037	0.0011	0.11
UFF	2.78	1.39	1.0	8.64	0.47	0.14

(i) a drastically higher degree of overlap $|\mathscr{O}|^2$, (ii) a larger transverse wavevector source extent $\mathscr{S}$, (iii) a lower value of d^2 (note that for a given choice of crystal, we have no control over d, which is angle dependent, with values $d = 1.64$ and $1.94\,\mathrm{pm\,V^{-1}}$ for the engineered and unengineered sources, respectively) and (iv) a smaller emitted bandwidth $\Delta\omega \equiv \Delta\omega_\mathrm{s} = \Delta\omega_\mathrm{i}$. Once we spectrally filter the unengineered source to make its degree of factorability (as quantified by the single-photon purity) equal to that of the engineered source (this corresponds to the UF source), the emitted bandwidth becomes much greater for the engineered source. The combined effect of the above explains the drastic brightness enhancement observed for the engineered source versus the UF source.

We now consider the UFF source, identical to the typical, spectrally filtered source except that: (i) the pump beam is focused to the same degree as for the engineered source and (ii) the fiber-collection mode radius is chosen to yield the maximum brightness for the selected degree of pump focusing. For this source, the pump bandwidth is $\Delta\lambda_\mathrm{pump} = 10.5\,\mathrm{nm}$, and the signal and idler modes are each transmitted through a filter with bandwidth 17.5 nm. The pump beam radius is $23.6\,\mu\mathrm{m}$, while the optimum brightness occurs for a fiber-collection mode radius of $11.4\,\mu\mathrm{m}$. While the advantage of the engineered source in terms of the emitted bandwidth basically remains, the advantage in terms of the degree of overlap is drastically reduced and the advantage in terms of the transverse wavevector extent is actually reversed. The engineered source requires larger propagation angles, with the effect of sharpening correlations involving transverse wavevectors (internal polar angle–frequency correlations and external azimuthal-angle correlations). This limits the enhancement in the degree of overlap over the typical, pump-focused, spectrally filtered source; the effect of the suppression of spatio-temporal entanglement observed for the engineered source is unfortunately offset by the effect of these sharpened transverse wavevector correlations. The net effect is that the engineered source has a brightness equal to ~ 0.47 of that of the UFF source.

Some recent works have demonstrated remarkably bright photon pair sources [37, 38]. For example, in [38], a considerably larger count rate per unit pump power and unit emission bandwidth is reported, compared to the UFF and engineered sources considered here. While Hentschel *et al* [38] report a brightness (here defined as pairs per second, normalized by pump power) close to $2 \times 10^5\,\mathrm{pairs\,s^{-1}\,mW^{-1}}$, our engineered source leads to a brightness close to $3 \times 10^3\,\mathrm{pairs\,s^{-1}\,mW^{-1}}$. In this experiment, however, no effort was made to render the photon pairs factorable. The situation is different when compared to sources designed to be factorable. Indeed, the rates of emission for the UFF and engineered sources studied in this paper are higher, compared to observed detection rates in a recent factorable photon pair generation experiment [16], which reports a brightness of $1.5 \times 10^2\,\mathrm{pairs\,s^{-1}\,mW^{-1}}$.

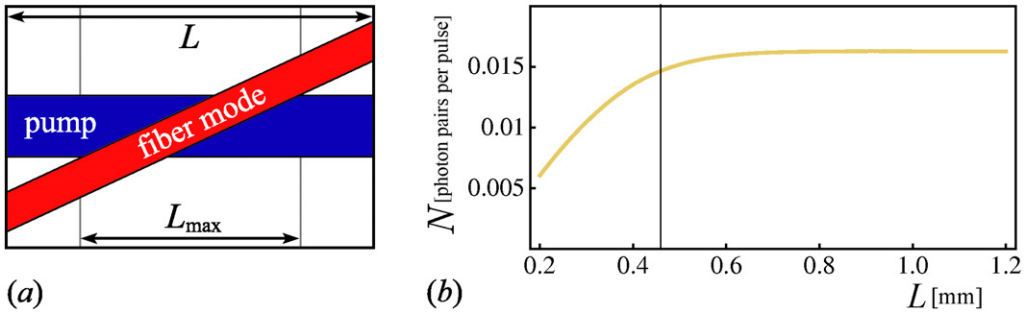

Figure 5. (a) Schematic of the fiber-collection mode (for one of the two photons), refracted into the crystal, together with the pump beam. (b) Emitted flux versus crystal length, showing saturation near $L = L_{max}$ (indicated by the thin vertical line).

In general terms, the attainable heralding efficiency is reduced by filtering—spatial or spectral—of the signal and idler modes. The UF and UFF sources involve spectral filtering, required in order to ensure factorability, and also involve spatial filtering associated with fiber coupling of the signal and idler modes. Although the engineered source does not involve spectral filtering, the transverse wavevector correlations (in particular, azimuthal–angle external correlations) resulting from the large propagation angles required for vector group velocity matching imply that the optimum fiber-collection modes lead to considerable spatial filtering. The heralding efficiency, computed numerically as N/N_s (see equations (25) and (26)), is 0.33 for the engineered source and 0.53 for the UFF source.

An important design consideration is the crystal length to be used. Generally, for SPDC, the flux dependence on crystal length tends to be linear. This is different in the present case where the signal and idler photon pairs, generated non-collinearly, are coupled into optical fiber. Figure 5(a) shows schematically the fiber-collection modes refracted from free space into the crystal and the pump beam (where we ignore the effects of diffraction). Only those photon pairs emitted into these intra-crystal fiber-collection modes can be coupled into the fibers. We can crudely estimate the length of crystal that can contribute to fiber-coupled photon pairs as the length of the overlap region between the pump beam and the intra-crystal fiber-collection modes. This leads to the following formula for the maximum effective crystal length, in terms of the internal orientation angle of the fiber modes θ:

$$L_{max} = \frac{\sqrt{2(w_f^2 + w_0^2 \cos^2\theta)}}{\sin\theta}. \tag{32}$$

This tells us that, within this simple model, increasing the crystal length beyond L_{max} does not result in any enhancement of the flux. Figure 5(b) shows the expected brightness (computed from equation (25)) versus crystal length for a source emitting at $\theta = 9.96^\circ$ with a pump beam radius of $w_0 = 40\,\mu$m and a fiber-collection mode radius of $w_f = 40\,\mu$m. The vertical line indicates the value of L_{max}, making it clear that around this value of the crystal length, the brightness reaches a plateau.

In the case of the engineered source, for a given crystal length the pump beam radius w_0 must have a specific value, determined by equation (14). From the plots in figure 6, we can then determine the value of the fiber-collection radius at the beamwaist w_f required for

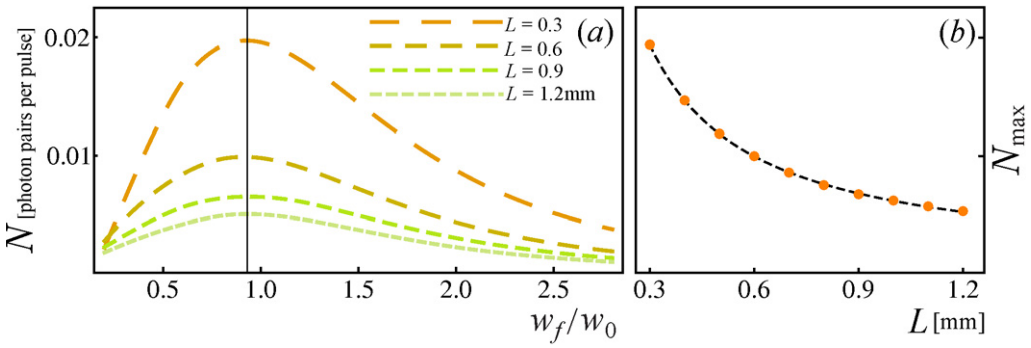

Figure 6. (a) Engineered source brightness versus w_f/w_0 for four different crystal lengths. Note that all four curves exhibit a maximum roughly at $w_f = 0.93 \times w_0$ (indicated by the vertical line). (b) Plot of the maximum brightness versus crystal length, calculated for $L = 0.3$, 0.6, 0.9 and 1.2 mm. The dashed line indicates a $1/L$ fit.

optimum fiber coupling. Figure 6(a) shows the expected brightness plotted versus the quotient w_f/w_0, for different crystal lengths. Note that the maximum occurs for an essentially fixed value of the quotient $w_f/w_0 \approx 0.93$ (the vertical line identifies this specific value of w_f/w_0), for all crystal lengths considered. Figure 6(b) shows the maximum brightness attainable as a function of crystal length, showing a $1/L$ dependence, valid within the range of values for the crystal length considered; the dotted line represents the best fit to a $1/L$ dependence. Of course, for short enough crystals, this trend will be reversed.

Interestingly, while the total flux varies linearly with crystal length, saturating to a plateau in the case of fiber coupling, the maximum *factorable* flux actually is greater for thinner crystals according to an $N \propto 1/L$ dependence. In order to understand this behavior, let us note that for the optimized geometry, as L is increased, w_0 must increase linearly with L (so as to fulfill equation (14)), and in turn w_f must increase linearly with w_0, so as to fulfill the condition $w_f/w_0 \simeq 0.93$, derived from figure 6. Therefore, because the angular extent of the two-photon state is inversely proportional to L and w_0, in order to ensure proper spatial modematching between the SPDC light and the fiber collection modes, the range of directions of propagation allowed to reach the detectors must be restricted in order to maintain factorability. Indeed, as we have pointed out, it is not possible to suppress ϕ_s–ϕ_i correlations, although they can be disregarded for a small enough spread of detected wavevectors. This is consistent with our condition 5 for factorability, which may be re-expressed in terms of the fiber collection mode radius w_f, using the relationship $\sin\Phi_{max} = 1/(kw_f)$. What this means, in practice, is that for longer crystals, the width of the azimuthal sector of the SPDC cone that one can detect for each of the two photons while maintaining factorability must decrease as L is increased, explaining the $1/L$ dependence of the maximum factorable flux. Note that a similar analysis carried out for the UFF source (not shown) indicates the same $1/L$ factorable flux behavior.

Even though in principle the factorable flux may be increased substantially by using progressively shorter crystals, in practice a shorter crystal leads to a larger phasematching bandwidth and, hence, to an increased pump bandwidth required to preserve factorability. This is consistent with our condition 4 for factorability, where the required bandwidth scales as $1/L$. Thus, in practice, the available pump bandwidth will limit how short the SPDC crystal can be made, and consequently will limit the attainable flux.

4. Conclusions

We have presented an analysis of the joint amplitude that characterizes photon pairs produced by non-collinear type-I SPDC. We have paid particular attention to the spatio-temporal correlations between the signal and idler photons, including both: (i) correlations between variables corresponding to different photons, which lead to quantum entanglement, and (ii) correlations between two variables corresponding to the same SPDC mode. This analysis is facilitated by writing an approximate version of the joint amplitude, expressed entirely in terms of Gaussian functions. Such a treatment leads to a specific set of conditions that permits the suppression of all spatio-temporal correlations between the signal and idler photons. We show that in order to guarantee factorability in cases where a spread of wavevectors is allowed to reach the detectors, it is essential to suppress correlations in all photonic degrees of freedom.

Exploiting our design criteria for the specific case of a BBO crystal, we verify through a numerical simulation, which does not resort to approximations, that the fulfillment of our conditions for factorability does in fact lead to a large brightness (defined as the number of fiber-coupled photon pairs per pump pulse), along with a high single heralded photon purity, indicating that the photon pairs are nearly factorable. This brightness enhancement is the result of engineering the two-photon state *at the source*, thus eliminating the need for filtering. We have also considered a different avenue towards bright, factorable photon pair sources: an unengineered source for which the pump beam is focused to the same degree as for the engineered source, for which the radius of the fiber-collection modes is selected so that the source brightness is optimized and for which factorability is ensured by spectral filtering. We find that the suppression of spatio-temporal entanglement observed for the engineered source is offset by the appearance of transverse wavevector correlations that cannot be made to vanish, with the effect that this last source has a brightness of the same order of magnitude as the engineered source. We have compared the expected brightness for the engineered and this unengineered, focused-pump, filtered source, with the expected brightness for an unengineered source, leading to a very considerable (two to three orders of magnitude) advantage over the unengineered source. Note that an engineered photon-pair source for which vector group velocity matching occurs for relatively small propagation angles would permit the full exploitation of the photon-pair engineering methods that we have developed. As a specific example, a frequency-degenerate photon-pair source based on a BBO crystal, configured for emission in the telecommunications band, leads to group velocity matching at comparatively small propagation angles. Note that for other types of crystals, shifting the emission wavelength towards the infrared likewise results in smaller vector group velocity matching angles. We expect that the analysis presented in this paper will be useful for the design of photon-pair sources tailored for quantum information processing applications.

Acknowledgments

This work was supported by: CONACYT, Mexico and DGAPA, UNAM (Mexico); FONCICYT project 94142; the European Commission (Qubit Applications, contract 015848); and the Government of Spain (Consolider Ingenio 2010 (QOIT) CSD2006-00019 and FIS2007-60179).

Appendix A

In order to describe the spatio-temporal correlations present in SPDC, it is convenient to write an approximate joint amplitude function entirely in terms of Gaussian functions. This can be achieved by approximating the sinc function in equation (7) as a Gaussian function with the same full-width at half-maximum, i.e. $\mathrm{sinc}(x) \approx \exp(-\gamma x^2)$ with $\gamma = 0.193$. The argument of the resulting Gaussian function can then be expressed as a first-order Taylor series in each of the six variables $\{\omega_\mathrm{s}, \theta_\mathrm{s}, \phi_\mathrm{s}, \omega_\mathrm{i}, \theta_\mathrm{i}, \phi_\mathrm{i}\}$, around corresponding central values. We define capital-letter variables corresponding to each of these six variables as the difference between each variable and its central value. The resulting expressions for a general orientation of the detection plane (i.e. for a general value of ϕ_0) tend to be complicated. Here we concentrate on the specific case $\phi_0 = 0$. We likewise assume that the pump beamwaist is located at the center of the crystal (i.e. $z_0 = 0$). In this case, the joint amplitude can be written in matrix form [39] as follows:

$$F(\Omega_\mathrm{s}, \Theta_\mathrm{s}, \Phi_\mathrm{s}; \Omega_\mathrm{i}, \Theta_\mathrm{i}, \Phi_\mathrm{i}) = \exp\left[-\tfrac{1}{2}\mathbf{X}\begin{pmatrix} t_{\mathrm{ss}}^2 & \tilde{\tau}_{\mathrm{ss}} & \tilde{T}_{\mathrm{ss}} & t_{\mathrm{si}}^2 & \tilde{\tau}_{\mathrm{si}} & \tilde{T}_{\mathrm{si}} \\ \tilde{\tau}_{\mathrm{ss}} & \alpha_{\mathrm{ss}} & \beta_{\mathrm{ss}} & \tilde{\tau}_{\mathrm{is}} & \alpha_{\mathrm{si}} & \beta_{\mathrm{si}} \\ \tilde{T}_{\mathrm{ss}} & \beta_{\mathrm{ss}} & \eta_{\mathrm{ss}} & \tilde{T}_{\mathrm{si}} & \beta_{\mathrm{si}} & \eta_{\mathrm{si}} \\ t_{\mathrm{si}}^2 & \tilde{\tau}_{\mathrm{is}} & \tilde{T}_{\mathrm{si}} & t_{\mathrm{ii}}^2 & \tilde{\tau}_{\mathrm{ii}} & \tilde{T}_{\mathrm{ii}} \\ \tilde{\tau}_{\mathrm{si}} & \alpha_{\mathrm{si}} & \beta_{\mathrm{si}} & \tilde{\tau}_{\mathrm{ii}} & \alpha_{\mathrm{ii}} & \beta_{\mathrm{ii}} \\ \tilde{T}_{\mathrm{si}} & \beta_{\mathrm{si}} & \eta_{\mathrm{si}} & \tilde{T}_{\mathrm{ii}} & \beta_{\mathrm{ii}} & \eta_{\mathrm{ii}} \end{pmatrix}\mathbf{X}^\mathrm{T}\right], \tag{A.1}$$

where $\mathbf{X}$ represents the row vector $(\Omega_\mathrm{s}\Theta_\mathrm{s}\Phi_\mathrm{s}\Omega_\mathrm{i}\Theta_\mathrm{i}\Phi_\mathrm{i})$ and $\mathbf{X}^\mathrm{T}$ represents the corresponding column vector. Here, we used the following definitions (with $l, m, \mu = \mathrm{s}, \mathrm{i}$):

$$t_{lm}^2 = 2\sigma^{-2} + \tfrac{1}{2}\gamma T_l T_m + \tfrac{1}{2}\tau_l \tau_m, \tag{A.2}$$

$$\alpha_{lm} = \tfrac{1}{2}\gamma L^2 k_{\perp l} k_{\perp m} + \tfrac{1}{2} w_0^2 k_{zl} k_{zm}, \tag{A.3}$$

$$\eta_{lm} = \tfrac{1}{2} k_{\perp l} k_{\perp m} (\gamma \rho^2 L^2 + w_0^2), \tag{A.4}$$

$$\tilde{\tau}_{lm} = \tfrac{1}{2}\gamma L T_l k_{\perp m} + \tfrac{1}{2} w_0 \tau_l k_{zm}, \tag{A.5}$$

$$\tilde{T}_{lm} = \tfrac{1}{2}\gamma L \rho k_{\perp l} T_m, \tag{A.6}$$

$$\beta_{lm} = \tfrac{1}{2}\gamma L^2 \rho k_{\perp l} k_{\perp m}, \tag{A.7}$$

and

$$T_\mu = L(k'_\mathrm{p}(\omega_{p0}) - k'_\mu(\omega_{\mu 0}\cos\theta_{\mu 0})), \tag{A.8}$$

$$\tau_\mu = w_0 k'_\mu(\omega_{\mu 0}) \sin\theta_{\mu 0}, \tag{A.9}$$

$$k_{z\mu} = k_\mu(\omega_{\mu 0}) \cos\theta_{\mu 0}, \tag{A.10}$$

$$k_{\perp\mu} = k_\mu(\omega_{\mu 0}) \sin\theta_{\mu 0}. \tag{A.11}$$

It can be inferred that for vanishing walk-off ($\rho = 0$), the resulting state is independent of the orientation of the detection plane [29] (characterized by angle ϕ_0). Because the effect of walk-off scales with crystal length, for relatively short crystals (such as those assumed in this paper), walk-off plays a limited role. In the case of experiments relying on longer crystals, it may be beneficial to use a specific detection plane. For example, from our analysis we have found that $\phi_0 = 90^\circ$ leads to exactly vanishing correlations involving the azimuthal angle variables and

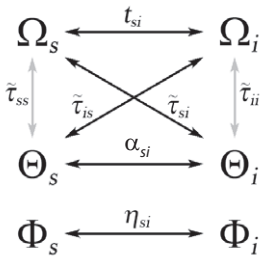

Figure A.1. Signal–idler photon pair correlations diagram for the spatial and spectral degrees of freedom, corresponding to vanishing pump walk-off. Dark lines represent the external (signal–idler) correlations, whereas light lines stand for internal (signal–signal or idler–idler) correlations.

walk-off-dependent polar angle/spectral correlation [29, 30]. This is in contrast with the $\phi_0 = 0^\circ$ case, for which correlations involving azimuthal angles do not vanish and polar angle/spectral correlations are walk-off independent. Figure A.1 represents schematically the correlations arising between the spatial and spectral degrees of freedom for the signal/idler photon pair, and the parameters that characterize these correlations, assuming vanishing walk-off of the pump field.

Elements along the diagonal of the matrix in equation (A.1) refer to widths (spectral or angular) for each of the photonic variables. Off-diagonal elements correspond to correlations between two variables. If we divide the matrix into four contiguous 3 by 3 blocks, then the two diagonal blocks refer to internal correlations, while the two off-diagonal blocks refer to external correlations. Since the matrix is symmetric, out of the 36 elements, at most 21 can be independent. For frequency-degenerate SPDC, only eight elements are independent as a consequence of the following relationships:

$$\begin{aligned} &T_\mathrm{s} = T_\mathrm{i} = T, \\ &\tau_\mathrm{s} = -\tau_\mathrm{i} = -\tau, \\ &k_{z\mathrm{s}} = k_{z\mathrm{i}} = k_z, \\ &k_{\perp\mathrm{s}} = -k_{\perp\mathrm{i}} = -k_\perp. \end{aligned} \tag{A.12}$$

In this case, (A.1) is reduced to

$$F(\Omega_\mathrm{s}, \Theta_\mathrm{s}, \Phi_\mathrm{s}; \Omega_\mathrm{i}, \Theta_\mathrm{i}, \Phi_\mathrm{i}) = \exp\left[-\tfrac{1}{2}\mathbf{X}\begin{pmatrix} t_+^2 & \tilde{\tau} & \tilde{T} & t_-^2 & -\tilde{\tau} & \tilde{T} \\ \tilde{\tau} & \alpha_+ & \beta & \tilde{\tau} & \alpha_- & -\beta \\ \tilde{T} & \beta & \eta & \tilde{T} & -\beta & -\eta \\ t_-^2 & \tilde{\tau} & \tilde{T} & t_+^2 & -\tilde{\tau} & -\tilde{T} \\ -\tilde{\tau} & \alpha_- & -\beta & -\tilde{\tau} & \alpha_+ & \beta \\ \tilde{T} & -\beta & -\eta & -\tilde{T} & \beta & \eta \end{pmatrix}\mathbf{X}^\mathrm{T}\right], \tag{A.13}$$

where

$$t_\pm^2 = 2\sigma^{-2} + \tfrac{1}{2}\gamma T^2 \pm \tfrac{1}{2}\tau^2, \tag{A.14}$$

$$\alpha_\pm = \pm\tfrac{1}{2}\gamma L^2 k_\perp^2 + \tfrac{1}{2}w_0^2 k_z^2, \tag{A.15}$$

$$\eta = \tfrac{1}{2}k_\perp^2(\gamma\rho^2 L^2 + w_0^2), \tag{A.16}$$

$$\tilde{\tau} = \tfrac{1}{2}\gamma L T k_\perp + \tfrac{1}{2} w_0 \tau k_z, \tag{A.17}$$

$$\tilde{T} = \tfrac{1}{2}\gamma L \rho k_\perp T, \tag{A.18}$$

$$\beta = \tfrac{1}{2}\gamma L^2 \rho k_\perp^2. \tag{A.19}$$

The conditions for factorability presented in this work were derived by imposing the condition that external correlation coefficients either vanish or are negligible simultaneously.

References

[1] Kok P, Munro W J, Nemoto K, Ralph T C, Dowling J P and Milburn G J 2007 *Rev. Mod. Phys.* **79** 135
[2] U'Ren A B, Silberhorn Ch, Banaszek K, Walmsley I A, Erdmann R, Grice W P and Raymer M G 2005 *Laser Phys.* **15** 146
[3] Santori C, Fattal D, Vuckovic J and Yamamoto Y 2002 *Nature* **419** 594
[4] Kurtsiefer C, Mayer C, Zarda P and Weinfurter H 2000 *Phys. Rev. Lett.* **85** 290
[5] Burnham D C and Weinberg D L 1970 *Phys. Rev. Lett.* **25** 84
[6] Fiorentino M, Voss P L, Sharping J E and Kumar P 2002 *Photon. Technol. Lett.* **14** 983
[7] Bouwmeester D, Pan J W, Daniell M, Weinfurter H and Zeilinger A 1999 *Phys. Rev. Lett.* **82** 1345
[8] Pan J W, Daniell M, Gasparoni S, Weihs G and Zeilinger A 2001 *Phys. Rev. Lett.* **86** 4435
[9] Zhao Z, Yang T, Chen Y A, Zhang A N, Zukowski M and Pan J W 2003 *Phys. Rev. Lett.* **91** 180401
[10] Eibl M, Gaertner S, Bourennane M, Kurtsiefer C, Zukowski M and Weinfurter H 2003 *Phys. Rev. Lett.* **90** 200403
[11] Zhao Z, Chen Y A, Zhang A N, Yang T, Briegel H J and Pan J W 2004 *Nature* **430** 54
[12] Lu C Y, Zhou X Q, Guhne O, Gao W B, Zhang W B, Zhang J, Yuan Z S, Goebel A, Yang T and Pan J W 2007 *Nat. Phys.* **3** 91
[13] Grice W P, U'Ren A B and Walmsley I A 2001 *Phys. Rev.* A **64** 063815
[14] Walton Z D, Sergienko A V, Saleh B E A and Teich M C 2004 *Phys. Rev.* A **70** 052317
[15] U'Ren A B, Erdmann R K, De la Cruz-Gutierrez M and Walmsley I A 2006 *Phys. Rev. Lett.* **97** 223602
[16] Mosley P J, Lundeen J S, Smith B J, Wasylczyk P, U'Ren A B, Silberhorn C and Walmsley I A 2008 *Phys. Rev. Lett.* **100** 133601
[17] Raymer M G, Noh J, Banaszek K and Walmsley I A 2005 *Phys. Rev.* A **72** 023825
[18] Kuzucu O, Fiorentino M, Albota M A, Wong F N C and Kärtner F X 2005 *Phys. Rev. Lett.* **94** 083601
[19] Hendrych M, Micuda M and Torres J P 2007 *Opt. Lett.* **32** 2339
[20] Garay-Palmett K, McGuiness H, Cohen O, Lundeen J, Rangel-Rojo R, U'Ren A B, Raymer M, McKinstrie C, Radic S and Walmsley I A 2007 *Opt. Express* **15** 14870
[21] Corona M and U'Ren A B 2007 *Phys. Rev.* A **76** 043829
[22] Kurtsiefer C, Oberparleiter M and Weinfurter H 2001 *Phys. Rev.* A **64** 023802
[23] Bovino F A, Varisco P, Colla A M, Castagnoli G, Di Giuseppe G and Sergienko A V 2003 *Opt. Commun.* **227** 343
[24] Trojek P, Schimd C, Bourennane M and Weinfurter C 2004 *Opt. Express* **12** 276
[25] Fedrizzi A, Herbst T, Poppe A, Jennewein T and Zeilinger A 2007 *Opt. Express* **15** 15377
[26] Law C K, Walmsley I A and Eberly J H 2000 *Phys. Rev. Lett.* **84** 5304
[27] U'Ren A B, Banaszek K and Walmsley I A 2003 *Quantum Inf. Comput. J.* **3** 480
[28] Valencia A, Cere A, Shi X, Molina-Terriza G and Torres J P 2007 *Phys. Rev. Lett.* **99** 243601
[29] Torres J P, Molina-terriza G and Torner L 2005 *J. Opt. B: Quantum Semiclass. Opt.* **7** 235
[30] Osorio C, Molina-Terriza G, Font B and Torres J P 2007 *Opt. Express* **15** 14636
[31] Dragan A 2004 *Phys. Rev.* A **70** 053814
[32] Kolenderski P, Wasilewski W and Banaszek K 2009 *Phys. Rev.* A **80** 013811

[33] Ling A, Lamas-Linares A and Kurtsiefer C 2008 *Phys. Rev.* A **77** 043834
[34] Aichele T, Lvovsky A I and Schiller S 2002 *Eur. Phys. J.* D **18** 237
[35] Kwait P G, Waks E, White A G, Appelbaum I and Eberhard P H 1999 *Phys. Rev.* A **60** R773
[36] Ljunggreen D and Tengner M 2005 *Phys. Rev.* A **72** 062301
[37] Krischek K, Wieczorek W, Ozawa A, Kiesel N, Michelberger P, Udem T and Weinfurter H 2010 *Nature Photon.* **4** 170
[38] Hentschel M, Hubel H, Poppe A and Zeilinger A 2009 *Opt. Express* **17** 23153
[39] Osorio C I, Valencia A and Torres J P 2008 *New J. Phys.* **10** 113012